Interplay of quadrupolar order, Ce 4f spin dynamics and RKKY induced conduction electron spin polarization in CeAg



2003 J. Phys.: Condens. Matter 15 8599

(http://iopscience.iop.org/0953-8984/15/49/030)

INSTITUTE OF PHYSICS PUBLISHING JOURNAL OF PHYSICS: CONDENSED MATTER

J. Phys.: Condens. Matter **15** (2003) 8599–8617 PII: S0953-8984(03)68784-9

# Interplay of quadrupolar order, Ce 4f spin dynamics and RKKY induced conduction electron spin polarization in CeAg

**A Schenck[1], F N Gygax[1], D Andreica[2] and Y Ōnuki[3]**

[1] Institute for Particle Physics of ETH Zürich, CH-5232 Villigen PSI, Switzerland
[2] Babes-Bolyai University, 3400 Cluj-Napoca, Romania
[3] Faculty of Science, Osaka University, Machikaneyama, Toyonaka, Osaka 560, Japan

Received 9 September 2003
Published 25 November 2003
Online at stacks.iop.org/JPhysCM/15/8599

**Abstract**

We report on measurements of the Knight shift $K$ and spin–lattice relaxation rate $\lambda$ of positive muons ($\mu^+$) implanted in cubic CeAg, a compound which is known to possess ferromagnetic ($T_c \simeq 5.5$ K) and ferroquadrupolar ($T_Q = 15$–$16$ K) order. The zero field (ZF) $\lambda$ implies randomly and isotropically fluctuating Ce 4f moments above $T_Q$ which show a trend to a, perhaps critical, slowing down on approaching $T_Q$. Below $T_Q$ the fluctuations are restricted to the now tetragonally distorted axis of CeAg. In a longitudinal field the generally isotropic fluctuations show a tendency towards freezing near $T_c$, not $T_Q$. The Knight shift results reveal an anisotropic contact hyperfine coupling parameter $A_c$, which displays abrupt changes at $T_c$. ZF measurements below $T_c$ reveal the presence of discrete spontaneous internal fields. The results on $\lambda$ and $A_c$ are interpreted as arising from quadrupolar effects, concerning in particular the induced spin polarization of the conduction electron system.

## 1. Introduction

Since the 1970s CeAg as well as other RX (R = Ce, Pr, Dy, Tm, X = Ag, Mg, Zn, Cu) compounds with cubic CsCl structure have attracted recurrent attention due to their rich magnetic and structural properties which are governed by one-ion magneto-elastic couplings and two-ion quadrupolar interactions [1]. CeAg, in particular, shows ferromagnetic order below $T_c \simeq 5.5$ K and a structural phase transition, driven by ferroquadrupolar order, at $T_Q = 15$–$16$ K. The latter changes the structure from cubic to tetragonal with $(a/c) - 1 \simeq 1.9\%$ (see [2], and references therein). The cubic crystalline electric field splits the $^2F_{5/2}$ multiplet of $Ce^{3+}$ into a $\Gamma_8$ quartet and an excited $\Gamma_7$ doublet. The tetragonal distortion leads to a splitting of the $\Gamma_8$ ground state into two doublets with expected moments of 2 and 0.429 $\mu_B$, respectively. The ferromagnetic state was investigated by neutron scattering yielding an ordered moment of $0.8 \pm 0.15$ $\mu_B$ at 1.8 K and $0.7 \pm 0.15$ $\mu_B$ at 4.3 K, presumably aligned along the tetragonal

  

*c*-axis [3]. From magnetization measurements the ordered moment was estimated to be in the range 0.7–1 $\mu_B$ [4, 5].

A multitude of techniques and procedures (substitution of La for Ce, and In for Ag, application of pressure, etc) have been used to study these properties in detail, but one important microscopic tool, namely nuclear magnetic resonance (NMR), has not been applied, probably because of the rather small nuclear moments of the two isotopes $^{107}$Ag and $^{109}$Ag of which natural silver is composed. An alternative related technique is provided by muon spin rotation/relaxation ($\mu$SR) spectroscopy [6] in which spin polarized positive muons are implanted interstitially and the time evolution of their polarization is monitored subsequently; this is similar to the free induction decay technique in NMR. This allows one to measure such quantities as the $\mu^+$ Knight shift and spin–lattice relaxation rates (also in zero applied field). Zero field (ZF) $\mu$SR measurements were indeed tried some years ago on polycrystalline samples [7], but the results were largely inconclusive, perhaps partly due to the limited time resolution available at the pulsed muon source and partly due to the chemical instability of CeAg and the history of the specimen used. Chemical instability and sample history have indeed plagued previous studies and have led to lack of reproducibility in part of the data [2].

More recently, high quality single crystals have become available, so even de Haas–van Alphen measurements have become possible [8]. Given this development, it appeared worthwhile to try once more to apply $\mu$SR to a study of the magnetic properties of CeAg on a microscopic scale. Using a new technique leads very often to the disclosure of new features and effects which have gone unnoticed in other studies. So in this work we report on new features which concern the spin dynamics of the Ce 4f electrons across $T_Q$ and $T_c$, and properties of the conduction electron spin polarization at the $\mu^+$ site which seem to be governed by the Ce 4f quadrupole moments.

## 2. Experimental details

As usual in a $\mu$SR experiment the evolution of the $\mu^+$ polarization $\boldsymbol{P}_\mu(t)$ is monitored via the time dependent decay asymmetry of the implanted $\mu^+$ by observing the positrons from the $\mu^+$ decay in a certain direction $\boldsymbol{r}$ as a function of elapsed $\mu^+$ lifetime. The positron rate can then be written as

$$\frac{\mathrm{d}N_{e^+}(t)}{\mathrm{d}t} = \frac{1}{4\pi\tau_\mu} N_0 \mathrm{e}^{-t/\tau_\mu}(1 - A\boldsymbol{P}_\mu(t)\cdot\boldsymbol{r})\,\mathrm{d}\Omega_r, \tag{1}$$

where $A$ is the effective decay asymmetry (0.2–0.3), $\tau_\mu$ the mean muon lifetime (2.2 $\mu$s), $|\boldsymbol{r}| = 1$ and $\mathrm{d}\Omega_r$ is a solid angle element in the direction of $\boldsymbol{r}$. In the following we will often call $AP_\mu(t) \equiv A\boldsymbol{P}_\mu(t)\cdot\boldsymbol{r}$ the asymmetry or signal amplitude.

The currently reported ZF, longitudinal field (LF) and transverse field (TF) $\mu$SR measurements were carried out with the general purpose spectrometer GPS on the $\pi$M3 beam line at PSI which provides 100% spin polarized $\mu^+$ with a momentum of 28 MeV/$c$ (so-called surface $\mu^+$). The instrument is equipped with a He-flow cryostat which allows one to set temperatures between 1.8 and 300 K. The positrons from the $\mu^+$ decay can be monitored in detectors placed forward, backward, up, down and to the right with respect to the $\mu^+$ beam axis or momentum. In the present experiment the initial $\mu^+$ beam polarization $\boldsymbol{P}_\mu(0)$ was rotated by approximately 45° from the horizontal-backward towards the vertical direction. An external field $H_{ext}$ up to 6 kOe can be applied parallel to the beam momentum. In the non-rotated case, $\boldsymbol{H}_{ext}$ and the initial $\mu^+$ polarization $\boldsymbol{P}_\mu(0)$ are parallel (the LF case) and no Larmor precession will occur, but the decay of $\boldsymbol{P}_\mu(t)$ due to relaxation processes can be monitored via the forward and backward positron rates. In the rotated case, $\boldsymbol{P}_\mu$ will precess around $\boldsymbol{H}_{ext}$ on the surface

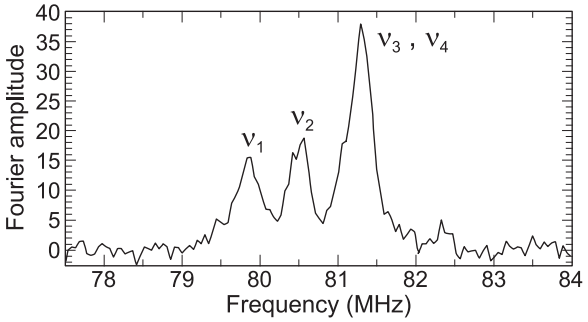


**Figure 1.** The Fourier transform of the TF $\mu$SR signal taken at 25 K. $\boldsymbol{H}_{\rm ext}$ is applied in a (001) plane and encloses an angle of 52° with the [100] axis. The dominant peak is actually composed of two narrowly spaced components $\nu_3$, $\nu_4$.

of a cone with an aperture of ∼90°. The precession can be monitored via the up, down and right positron rates. The component of $\boldsymbol{P}_\mu(0)$ along $\boldsymbol{H}_{\rm ext}$ does not take part in the Larmor precession but may again decay due to some relaxation mechanism, observable in forward and backward directions simultaneously with the precession signal in the up, down and right directions.

The single crystal used was grown at Osaka University [8] and had approximately the shape of a cylinder with 2.7 mm diameter and 3.6 mm length. The cylinder axis coincided with a [001] axis. It was mounted on a tube made from Mylar foil with negligible mass so that practically no $\mu^+$ were stopped in the sample holder. Muons passing around the sample and their decay positrons were largely vetoed out by a clever detector arrangement. The sample could be rotated around the sample holder axis, coinciding with one of the cubic axes, i.e. perpendicular to the beam momentum so that $\boldsymbol{P}_\mu(0)$ or $\boldsymbol{H}_{\rm ext}$ would turn in one of the corresponding planes (e.g. (100)).

## 3. Measurements in transverse field

### *3.1. Presentation of results*

All measurements were performed in an applied field of 6 kOe. Figure 1 displays the Fourier transform of the $\mu$SR spectrum taken at 25 K with $\boldsymbol{H}_{\rm ext}$ in the (001) plane, and enclosing an angle of 52° with the [100] axis. We notice three peaks. The peak to the right is actually composed of two frequencies as the further analysis shows. Hence the time evolution of the $\mu^+$ polarization in the up, down and right directions is perfectly fitted by the four component expression

$$P(t) = \sum_{i=1}^{4} A_i \mathrm{e}^{-\lambda_{{\rm TF},i}t} \cos(\omega_i t). \tag{2}$$

Each component relaxes effectively exponentially. In the actual analysis a fifth component, representing those $\mu^+$ which had stopped outside of the sample, was taken into account. This component contributes less than 5% to the precession signal.

The four frequencies were followed as a function of the orientation of $\boldsymbol{H}_{\rm ext}$ in the (001) plane at 25 K. The results are displayed in figure 2. Two of the frequencies show no orientation dependence while the pair $\nu_1$, $\nu_2$ follows a $\cos^2(\theta)$ dependence with a relative phase shift of 90°. As regards the amplitudes $A_i$ we find $A_1 = A_2 = A_3 \simeq 0.29A_{\rm max}$ and $A_4 \simeq 0.13A_{\rm max}$,

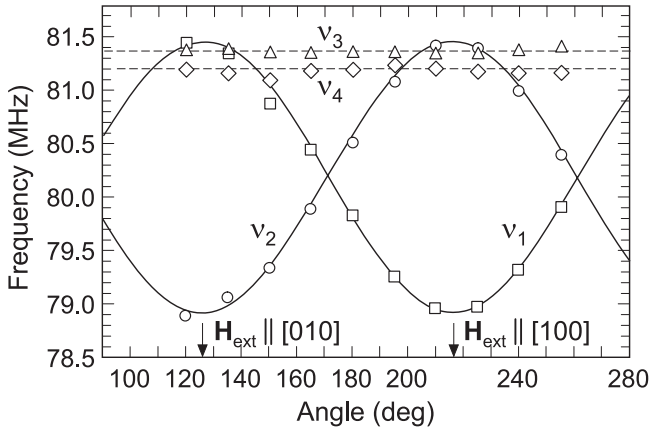


**Figure 2.** The orientation dependence of $\nu_1$, $\nu_2$, $\nu_3$ and $\nu_4$ at 25 K when $\boldsymbol{H}_{\rm ext}$ is rotated in a (001) plane. Note the clear splitting of the $\nu_i$ for $\boldsymbol{H}_{\rm ext} \parallel [100]$ or $\parallel[110]$.

where $A_{\rm max}$ is the total decay asymmetry. Note that for $\boldsymbol{H}_{\rm ext} \parallel [100]$, $\nu_2$, $\nu_3$ and $\nu_4$ do not coincide. The consequences of this behaviour will be discussed in the next section.

The temperature dependence of the $\nu_i$ for $\boldsymbol{H} \parallel [100]$ between 6 and 250 K is displayed in figures 3(a), (b). Above 120 K all four components collapse onto a single line, indicating the onset of long range $\mu^+$ diffusion in this compound. Note the huge negative shift of $\nu_1$ at low temperatures (figure 3(a) inset). For completeness figure 4 shows the temperature dependence of the $\lambda_{{\rm TF},i}$ $(i = 1, 2, 3)$. The increase around 120 K is a typical phenomenon when the $\mu^+$ start to hop between different local fields [9]. We will see in section 5 that the relaxation rate in the LF configuration is of similar magnitude and follows a similar trend with temperature. This implies that the $\lambda_i$ $(i = 1, 2, 3)$ are not reflecting static field inhomogeneities but dynamically induced relaxation, and hence $\lambda_i$ may be viewed as a spin–spin relaxation rate $(1/T_{2,i})$ [10].

### *3.2. Discussion of TF results*

*3.2.1. Angular dependence.* The angular dependence of the $\nu_i$ reflects the anisotropy of the $\mu^+$ Knight shifts. Other contributions to the local field, i.e. the demagnetization and Lorentz fields, are independent of orientation since, firstly, the sample was rotated around its cylinder axis and, secondly, the bulk magnetic susceptibility is isotropic. The anisotropy may arise from both the dipolar fields from the induced moments on the Ce sites and the contact hyperfine field at the $\mu^+$ site [11]. The observation that $A_1 = A_2 = A_3$ suggests that the three components are associated with the same crystallographic but magnetically inequivalent sites. Moreover the fact that $\nu_3$ is orientation independent implies that the relevant dipolar coupling tensor contains only diagonal elements and is axially symmetric. Inspecting the crystal structure of CeAg (see figure 5), only two types of interstitial site appear reasonable, namely the c and d sites (Wyckoff notation), each associated with multiplicity 3. All other possible sites (e.g. e, f, g) can be excluded since they do not admit an orientation independent $\nu_3$. For the c and d sites the associated traceless dipolar coupling tensors $(A_{ij}^{\rm dip})$ are diagonal and axially symmetric with respect to one of the crystal axes. Calculated $A_{ii}^{\rm dip}$ are collected in table 1 for both the c and d sites.

In the present experiment the external field $\boldsymbol{H}_{\rm ext}$ was rotated in the (001) plane, i.e. $\boldsymbol{H}_{\rm ext} = H[\cos\varphi, \sin\varphi, 0]$. The angular dependence of the fractional frequency shift (or Knight shift)

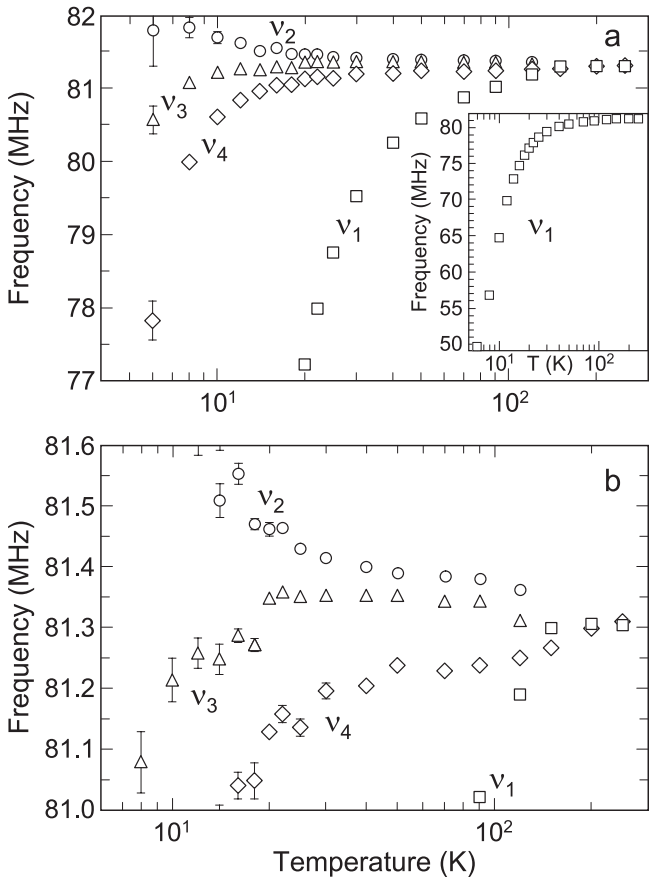


**Figure 3.** The temperature dependence of $\nu_i$ ($i = 1, 2, 3, 4$) for $\boldsymbol{H}_{\rm ext} \parallel [100]$. The inset in (a) shows the full variation of $\nu_1$, while in (b) the $\nu_i$ are shown on an extended vertical scale.

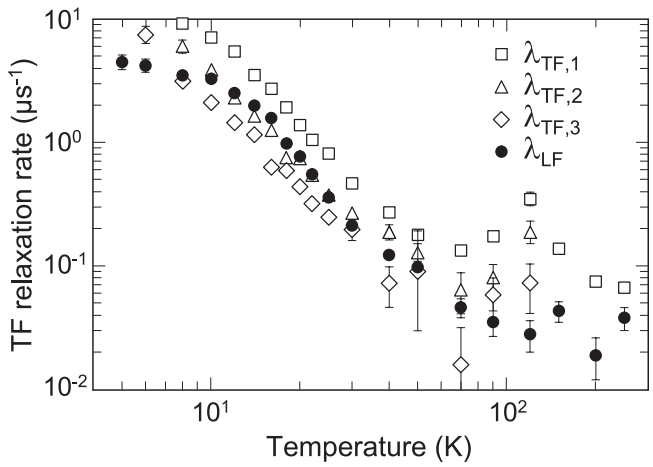


**Figure 4.** The temperature dependence of $\lambda_{{\rm TF},i}$ ($i = 1, 2, 3$) and that of $\lambda_{\rm LF}$.

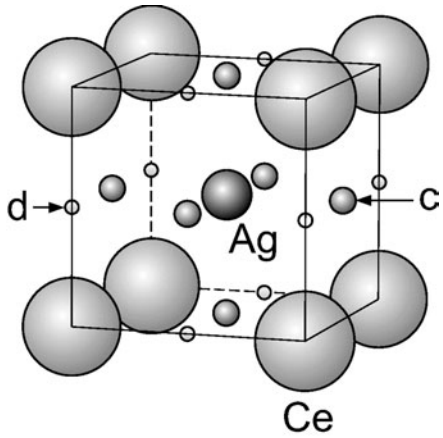


**Figure 5.** The crystal structure of cubic CeAg with the 3c and 3d sites indicated.

**Table 1.** A compilation of calculated dipolar coupling constants (kG/$\mu_B$) for cubic[a] and tetragonally distorted[b] CeAg. The $x, y, z$ axes correspond to the crystal axes [100], [010], [001].

| | | Cubic | | | Tetragonal | | |
|---|---|---|---|---|---|---|---|
| No | Site | $A_{xx}$ | $A_{yy}$ | $A_{zz}$ | $A_{xx}$ | $A_{yy}$ | $A_{zz}$ |
| | c | | | | | | |
| 1 | $(0\frac{1}{2}\frac{1}{2})$ | −1.528 | 0.764 | 0.764 | −1.496 | 0.704 | 0.792 |
| 2 | $(\frac{1}{2}0\frac{1}{2})$ | 0.764 | −1.528 | 0.764 | 0.704 | −1.496 | 0.792 |
| 3 | $(\frac{1}{2}\frac{1}{2}0)$ | 0.764 | 0.764 | −1.528 | 0.788 | 0.788 | −0.577 |
| | d | | | | | | |
| 1 | $(\frac{1}{2}00)$ | 5.288 | −2.644 | −2.644 | 5.361 | −2.666 | −2.695 |
| 2 | $(0\frac{1}{2}0)$ | −2.644 | 5.288 | −2.644 | −2.666 | 5.361 | −2.695 |
| 3 | $(00\frac{1}{2})$ | −2.644 | −2.644 | 5.288 | −2.522 | −2.522 | 5.044 |

[a] $a = b = c = 3.756$ Å.
[b] $a = b = 3.739$ Å, $c = 3.811$ Å [8].

$\Delta\nu_i/\nu_{ext} = (\nu_i - \nu_{ext})/\nu_{ext} = K_i$, neglecting at first a contact field contribution, is then given by [11]

$$K_i(\varphi) = \tfrac{1}{2}[A^{dip}_{xx,i} + A^{dip}_{yy,i} + (A^{dip}_{xx,i} - A^{dip}_{yy,i})\cos 2\varphi]\chi, \tag{3}$$

where $\nu_{ext} = \gamma_\mu H_{ext}$ ($\gamma_\mu = 2\pi \times 13.55$ kHz G$^{-1}$); $x, y, z$ refer to the crystal axes [100], [010], [001] and $\chi$ is the magnetic (bulk) susceptibility. Equation (3) does indeed describe correctly the angular behaviour of the frequencies $\nu_1, \nu_2, \nu_3$ with the same amplitudes. Hence $\nu_1$ may be associated with e.g. the c site $(0\frac{1}{2}\frac{1}{2})$, $\nu_2$ with $(\frac{1}{2}0\frac{1}{2})$ and $\nu_3$ with $(\frac{1}{2}\frac{1}{2}0)$, the latter showing no angular dependence. However, according to this scheme for $\varphi = 0$, $K_2 = K_3$. This is clearly not observed as figures 2 and 3 demonstrate, and the sites $(\frac{1}{2}0\frac{1}{2})$ and $(\frac{1}{2}\frac{1}{2}0)$ are not equivalent for $\varphi = 0$.

The inequivalence may be attributed either to a lattice distortion or to the contact hyperfine field, so far not considered. As regards the first possibility, one may speculate that above $T_Q$ a small tetragonal distortion is already present. Table 1 lists calculated $A^{dip}_{ii}$ for this case, based on the low temperature tetragonal distortion. As expected, $A^{dip}_{xx}$ becomes different for e.g. the c sites $(\frac{1}{2}\frac{1}{2}0)$ and $(\frac{1}{2}0\frac{1}{2})$. So, a tetragonal distortion could explain in principle the splitting of $\nu_2$ and $\nu_3$ for $\varphi = 0°$, but would leave the angular behaviour unchanged.

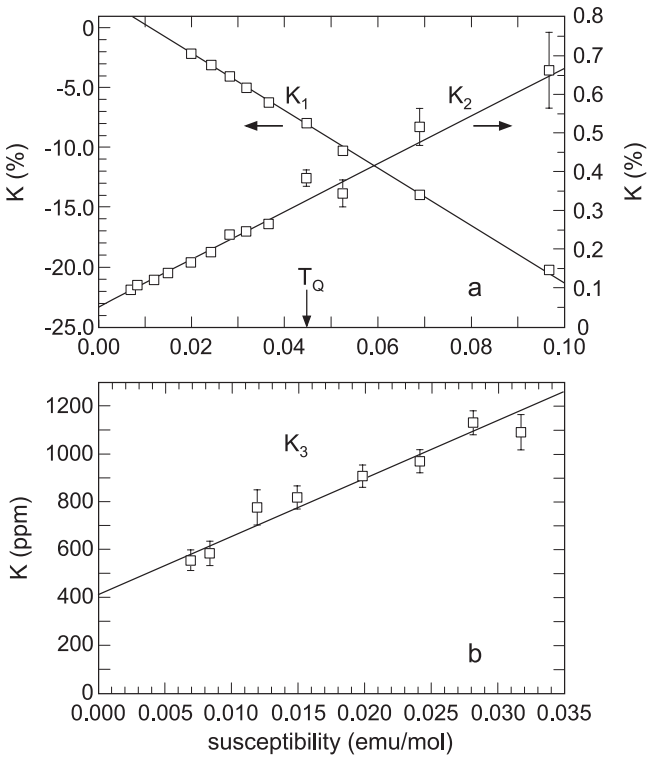


**Figure 6.** Plots of Knight shift versus susceptibility (Clogston–Jaccarino plot), (a) $K_1$, $K_2$; (b) $K_3$. $\boldsymbol{H}_{\rm ext} \parallel [100]$; the susceptibility data are taken from [2] and [5].

The fourth frequency $\nu_4$, showing no orientation dependence, and no further splitting, is not compatible with any assignment to a regular interstitial site. We conjecture that it can be attributed to $\mu^+$ located at a defect site, e.g. at a vacancy in the Ag sublattice. Such sites also possess locally cubic symmetry and the dipole fields from the Ce sublattice will cancel at these sites. The Knight shift $K_4$ extracted from $\nu_4$ should then only be caused by the contact hyperfine field.

*3.2.2. Temperature dependence.* Next we consider the temperature dependence of the Knight shifts $K_i$ for $\varphi = 0°$, extracted from $\nu_1$, $\nu_2$ and $\nu_3$ after proper corrections for the demagnetization and Lorentz fields have been applied. Comments on $\nu_4$ will be presented at the end of this section. According to equation (3), $K_i$ should scale with the susceptibility $\chi$. This is indeed observed below the temperature range where $\mu^+$ diffusion appears to set in. More precisely $K_1$ scales with the bulk $\chi$ between 10 and 30 K, $K_2$ between 10 and 90 K (see figure 6(a)) and $K_3$ between 20 and 90 K (see figure 6(b)). The fitted slopes $\mathrm{d}K/\mathrm{d}\chi$ are collected in table 2. Note that the slopes of $K_1$ and $K_2$ are not affected by the transition at $T_{\rm Q}$.

We now have to take into account also the contact hyperfine contribution. We then write [11]

$$\mathrm{d}K_i(\varphi)/\mathrm{d}\chi = A_{{\rm c},i}(\varphi) + \tfrac{1}{2}(A^{\rm dip}_{xx,i} + A^{\rm dip}_{yy,i} + (A^{\rm dip}_{xx,i} - A^{\rm dip}_{yy,i})\cos 2\varphi). \qquad (4)$$

Usually it is assumed that the contact coupling constant $A_{\rm c}$ is isotropic and temperature independent, i.e. $A_{\rm c}$ is the same for all c sites and for all d sites. As we shall see, this cannot be

**Table 2.** A collection of fitted $dK_i/d\chi$ and extracted $A_c$ for $\boldsymbol{H}_{ext} \parallel [100]$ ($\varphi = 0$).

| Signal | Site | $dK_i/d\chi$ | $A_c$ (kG/$\mu_B$)[a] |
|---|---|---|---|
| $\nu_1$ | $(0\frac{1}{2}\frac{1}{2})$ | −13.39 (4) | −11.86 |
| $\nu_2$ | $(\frac{1}{2}0\frac{1}{2})$ | +0.344 (12) | −0.360 |
| $\nu_3$ | $(\frac{1}{2}\frac{1}{2}0)$ | +0.136 (10) | −0.652 |

[a] Cubic structure assumed.

the case for CeAg. Other examples of anisotropic and temperature dependent $A_c$ were found in $U_{0.965}Th_{0.035}Be_{13}$ [12], $UPd_3$ [13], $HoB_2C_2$ [14] and, more recently, $Ce_{1-x}La_xB_6$ [15]. For $\varphi = 0$ equation (4) reduces for the 3c or d subsites to

$$dK_1/d\chi = A_{c,1} + A^{dip}_{xx,1} = A_{c,1} - 2A^{dip}_{xx}, \tag{5a}$$

$$dK_2/d\chi = A_{c,2} + A^{dip}_{xx,2} = A_{c,2} + A^{dip}_{xx}, \tag{5b}$$

$$dK_3/d\chi = A_{c,3} + A^{dip}_{xx,3} = A_{c,3} + A^{dip}_{xx}, \tag{5c}$$

with $A^{dip}_{xx} \equiv A^{dip}_{xx,2}$ (see table 1). Assuming further that $A_{c,1} = A_{c,2} = A_{c,3}$ and noting that $K_2(0°) = K_1(90°)$ we combine

$$dK_1/d\chi = -13.39\ \text{kG}/\mu_B = A_c - 2A^{dip}_{xx}, \tag{6a}$$

and

$$dK_2/d\chi = 0.344\ \text{kG}/\mu_B = A_c + A^{dip}_{xx}, \tag{6b}$$

and arrive at $A^{dip}_{xx} = +4.23$ kG/$\mu_B$ and $A_c = -8.81$ kG/$\mu_B$. Comparing this $A^{dip}_{xx}$ value with the entries in table 1, it becomes clear that the assumption of an isotropic $A_c$ cannot be correct and leads to impossible values for $A^{dip}_{xx}$, given that only the c or d sites can be involved. Of course, it is now impossible to decide unambiguously which of the two interstitial sites is occupied. However, we think that the c site is more likely as it allows the $\mu^+$ to stay as far as possible away from the $Ce^{3+}$ ions, while the Coulomb forces between the $\mu^+$ and $Ag^+$ ions are less strong. In the following we will therefore restrict the discussion to an occupation of the c site.

Hence we assume that the calculated $A^{dip}_{ii}$ values for the c sites are the proper values. It is then possible to extract $A_{c,i}$ from the $dK_i/d\chi$. $A_c$ will be anisotropic but temperature independent at least within the temperature range in which $K_i$ scales with $\chi$. The extracted values for $A_{c,i}$ are also collected in table 2 and in figure 7 for the cubic and tetragonal structure. Below the scaling regime, $A_{c,i}$ is extracted from $K_i$ assuming that the local susceptibility is still correctly given by the bulk susceptibility $\chi$. As figure 7 shows, $A_{c,1}$ becomes strongly temperature dependent below 10 K, while $A_{c,2}$ and $A_{c,3}$ are rather temperature independent. A further abrupt change occurs below $T_c$ (see section 4.2). We note that the $A_c$ derived from $K_2$ and $K_3$ are also significantly different. This raises the suspicion that the splitting of $\nu_2$ and $\nu_3$ for $H_{ext} \parallel [100]$ may arise primarily from the anisotropy of $A_c$ and not be caused by a tetragonal distortion of CeAg, which, anyway, above $T_Q$, has not been evidenced by any other technique.

Finally we mention that the Knight shift $K_4$ extracted from $\nu_4$ scales with $\chi$ between 20 and 100 K with a slope $dK_4/d\chi = 0.17\ \text{kG}/\mu_B$. If the $\mu^+$ contributing to $\nu_4$ are indeed located at a vacancy in the Ag sublattice, then $dK_4/d\chi$ is given by just the contact coupling constant $A_{c,\nu_4}$ associated with this site. Below 20 K, $A_{c,\nu_4}$ becomes temperature dependent and assumes at 6 K an approximate value of $-0.32$ kG/$\mu_B$.

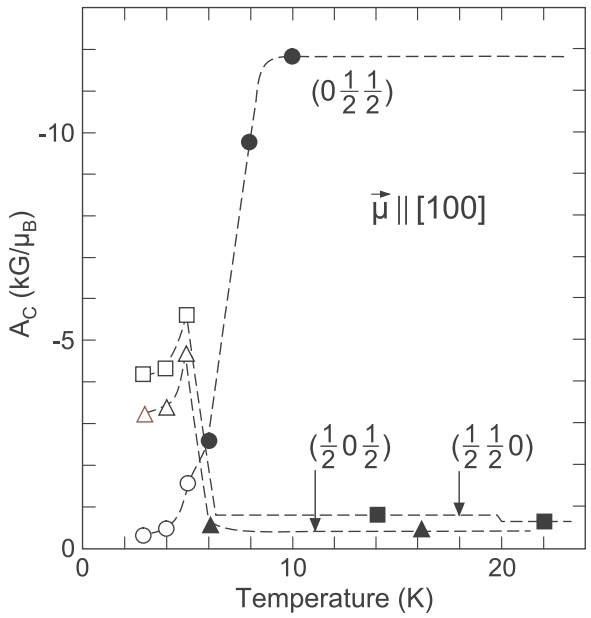


**Figure 7.** The temperature dependence of the contact coupling constant $A_c$ at the different c sites and with the induced or ordered moment ‖[100]. The values for $T < T_c$ (open symbols) are derived from the spontaneous $B_i$, the values for $T > T_c$ from the $K_i$ (filled symbols and dashed lines).

*3.2.3. Anisotropy of $A_c$.* Inclusion of the contact hyperfine field contribution in equation (4) should not alter the orientation dependence of the $K_i$, which was perfectly accounted for by equation (3). This can be accomplished by adopting the phenomenological expression

$$A_c = \sum_{i=1}^{4} \sin^2\theta_i(\cos^2(\phi_i)A^c_{x'x'} + \sin^2(\phi_i)A^c_{y'y'}) + \cos^2(\theta_i)A^c_{z'z'}, \tag{7}$$

where the polar coordinates refer to a coordinate system with the $z'$-axis parallel to [001] and the $x'$-axis parallel to $\boldsymbol{H}_{ext}$; i.e., we postulate that the 'object', described by equation (7), follows the field or the induced moment on the Ce sites ($\boldsymbol{\mu} = \chi \cdot \boldsymbol{H}_{ext}$). The angles $\theta$ and $\phi$ determine the direction angles of the distance vector connecting the $\mu^+$ and one of the nearest Ce neighbours. The sum in equation (7) is restricted to the four nearest Ce neighbours around the $\mu^+$.

The dependence on $\varphi$ of $A_c$ can then be expressed for the 3c sites as follows. For $(\frac{1}{2}\frac{1}{2}0)$: $\theta_i = 90°$, $\phi_{1,2} = 45° - \varphi$, $\phi_{3,4} = 45° + \varphi$,

$$\begin{aligned} A_c(\varphi) &= 2[A^c_{x'x'}\cos^2(45° - \varphi) + A^c_{y'y'}\sin^2(45° - \varphi) + A^c_{x'x'}\cos^2(45° + \varphi) \\ &\quad + A^c_{y'y'}\sin^2(45° + \varphi)] = 2(A^c_{x'x'} + A^c_{y'y'}). \end{aligned} \tag{8a}$$

For $(\frac{1}{2}0\frac{1}{2})$: $\theta_1 = 45°$, $\theta_2 = -45°$, $\theta_3 = 135°$, $\theta_4 = -135°$, $\phi_i = -\varphi$,

$$\begin{aligned} A_c(\varphi) &= 4[A^c_{z'z'}\cos^2(45°) + (A^c_{x'x'}\cos^2\varphi + A^c_{y'y'}\sin^2\varphi)\sin^2(45°)] \\ &= 2[A^c_{z'z'} + A^c_{y'y'} + (A^c_{x'x'} - A^c_{y'y'})\cos^2\varphi] \\ &= 2A^c_{z'z'} + A^c_{y'y'} + A^c_{x'x'} + (A^c_{x'x'} - A^c_{y'y'})\cos 2\varphi. \end{aligned} \tag{8b}$$

For $(0\frac{1}{2}\frac{1}{2})$: $\theta_1 = 45°$, $\theta_2 = -45°$, $\theta_3 = 135°$, $\theta_4 = -135°$, $\phi_i = 90° - \varphi$,

$$\begin{aligned} A_c(\varphi) &= 2[A^c_{z'z'} + A^c_{x'x'} + (A^c_{y'y'} - A^c_{x'x'})\cos^2\varphi] \\ &= 2A^c_{z'z'} + A^c_{y'y'} + A^c_{x'x'} + (A^c_{y'y'} - A^c_{x'x'})\cos 2\varphi. \end{aligned} \tag{8c}$$

**Table 3.** A compilation of spontaneous frequencies $\nu_i$, internal fields $B_i$, extracted hyperfine fields at 3 K and site assignments considered.

| Signal $i$ | $\nu_i$ (MHz) | $B_i$ (kG) | $B_{\rm dip} + B_{\rm c}$ (kG) | $B_{\rm c}$ (kG)[a] | Site |
|---|---|---|---|---|---|
| 1 | 11.79(13) | ±0.87(7) | <u>+0.145</u>, −1.59 | −0.64(1) | Ag vacancy |
| 2 | 14.47(26) | ±1.07(22) | +0.345, <u>−1.795</u> | −0.30(2) | $(0\frac{1}{2}\frac{1}{2})$ |
| 3 | 24.21(7) | ±1.79(5) | +1.065, <u>−2.515</u> | −3.22(1) | $(\frac{1}{2}0\frac{1}{2})$ |
| 4 | 36.42(26) | ±2.69(22) | +1.965, <u>−3.415</u> | −4.20(2) | $(\frac{1}{2}\frac{1}{2}0)$ |

[a] $B_{\rm c}$ is obtained by using the underlined values for $B_{\rm dip} + B_{\rm c}$ and calculated $B_{\rm dip}$ for the site considered from table 1 and $\mu = 1\ \mu_{\rm B}$.

**Table 4.** A compilation of the estimated coupling parameters in equation (7) (kG/$\mu_{\rm B}$).

| | $T \geqslant 10$ K | $T \lesssim 3$ K |
|---|---|---|
| $A^{\rm c}_{x'x'}$ | −2.913 | −1.78 |
| $A^{\rm c}_{y'y'}$ | −3.017 | −0.32 |
| $A^{\rm c}_{z'z'}$ | 2.703 | +0.17 |

Hence $A_{\rm c}(\varphi)$ can be written completely analogously to equation (3). In particular, the orientation independence of $\nu_3$ is retained. At $\varphi = 0$ we obtain (see table 2)

$$\text{at } (\tfrac{1}{2}\tfrac{1}{2}0) \qquad A_{{\rm c},1}(0) = 2(A^{\rm c}_{x'x'} + A^{\rm c}_{y'y'}) = -11.86\ {\rm kG}/\mu_{\rm B},$$
$$\text{at } (\tfrac{1}{2}0\tfrac{1}{2}) \qquad A_{{\rm c},2}(0) = 2(A^{\rm c}_{z'z'} + A^{\rm c}_{x'x'}) = -0.42\ {\rm kG}/\mu_{\rm B},$$
$$\text{at } (0\tfrac{1}{2}\tfrac{1}{2}) \qquad A_{{\rm c},3}(0) = 2(A^{\rm c}_{z'z'} + A^{\rm c}_{y'y'}) = -0.628\ {\rm kG}/\mu_{\rm B},$$

i.e., the splitting of $\nu_2$ and $\nu_3$ is reproduced and we obtain $A^{\rm c}_{x'x'} = -2.913$ kG/$\mu_{\rm B}$, $A^{\rm c}_{y'y'} = -3.017$ kG/$\mu_{\rm B}$, $A^{\rm c}_{z'z'} = +2.703$ kG/$\mu_{\rm B}$, also listed in table 4. Thus it is not necessary to invoke a tetragonal distortion of CeAg above $T_{\rm Q}$ in order to explain the splitting of $\nu_2$ and $\nu_3$.

A justification of equation (7) may be given as follows. The contact hyperfine fields originate from the conduction electron spin polarization at the $\mu^+$ which is induced by the local Ce moments via the Ruderman–Kittel–Kasuya–Yosida (RKKY) mechanism [11]. Accordingly, $A_{\rm c}$ is proportional to the overlap (or exchange) integral of the aspherical 4f electron distribution (characterized by a non-zero quadrupole moment) and the more or less spherical conduction electron screening cloud around the $\mu^+$. Therefore the overlap integral is expected to depend strongly on the relative orientation of the aspherical 4f electron distribution and the inhomogeneously distributed conduction electrons in the vicinity of the $\mu^+$ [13]. The general form of equation (7) may in a sense reflect the aspherical 4f electron distribution. Our model implies that it is rigidly coupled to the direction of the field induced magnetic moment on the Ce sites and has a definite orientation with respect to the [001] axis. The former implies a very strong $LS$ coupling, the latter the influence of the crystalline electric field (CEF). The origin of the different signs of the extracted $A^{\rm c}_{i'i'}$ is less clear. We conjecture that it arises from the spatially oscillatory behaviour of the RKKY induced conduction electron spin polarization and could point to effective Fermi momenta which are different for inequivalent directions.

## 4. Measurements in zero field

Generally the [100] crystal axis was oriented parallel to the $\mu^+$ beam momentum.

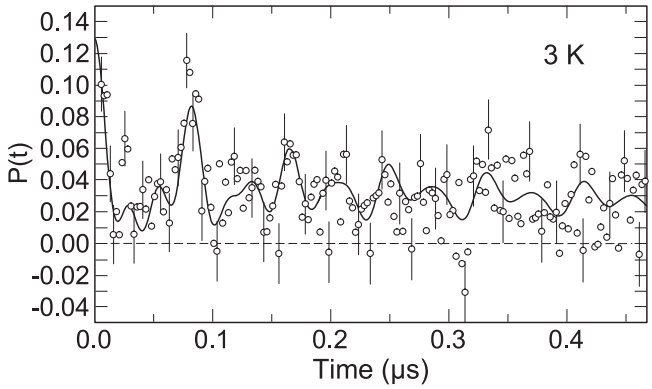


**Figure 8.** The time dependence of the $\mu^+$ polarization $P_\mu(t)$ observed in the 'down' direction at 3 K. The solid curve represents a fit of equation (9) to the data. Note that the initial $\boldsymbol{P}_\mu(0)$ is rotated by 45° from the beam axis towards the vertical direction.

### *4.1. The ferromagnetic phase ($T < 5.5$ K)*

Only three temperature settings (3, 4, 5 K) could be studied but the information carried by them is sufficiently rich to be reported here.

The signals observed in the up, down, forward and backward directions revealed four spontaneous frequencies and one relatively slowly and exponentially decaying component. The presence of four frequencies was extracted by admitting in the fit procedure first one, then two etc frequencies. Accordingly the time evolution of the $\mu^+$ polarization was best fitted by the expression

$$P(t) = \sum_{i=1}^{4} A_i \exp(-\lambda_1 t) \cos 2\pi \nu_i t + A_5 \exp(-\lambda_5 t). \tag{9}$$

The signal obtained at 3 K in the down detector and the fitted $P(t)$ are displayed in figure 8 for the early part of the spectrum.

We found that $A_1 \simeq A_2 \simeq A_3 \simeq A_4$ and $\sum_{i=1}^{5} A_i = A_{\mathrm{tot}}$, where $A_{\mathrm{tot}}$ is the maximum possible asymmetry observed above $T_c$. Further, $A_5 \simeq \frac{1}{3} A_{\max}$.

In the final fit we used the restriction $A_4 = A_3 = A_2 = A_1$. The temperature dependences of the fitted $\nu_1$ and $\lambda_i$ are displayed in figures 9 and 10. The observation of four frequencies or four different internal fields with more or less equal weight finds its analogue in the observation of a fourfold split TF precession signal above $T_c$, suggesting that three of the frequencies are associated with the three magnetically inequivalent c sites and the fourth frequency with some defect site, e.g. the suggested vacancy in the Ag sublattice. The fifth component, to which about $1/3$ of the implanted $\mu^+$ contribute, arises from those $\mu^+$ spins which are parallel to the internal field and, hence, do not precess (the so-called $1/3$ component). This component will show depolarization if fluctuating field components perpendicular to the spin are present, causing spin–lattice relaxation. For randomly oriented static internal fields, which are expected in CeAg due to the multidomain structure, one can show that $1/3$ of all implanted $\mu^+$ do indeed contribute to this component. $\lambda_5$ changes from 0.8 $\mu s^{-1}$ at 3 K to 0.53 $\mu s^{-1}$ at 5 K.

### *4.2. Discussion of the results for the ferromagnetic phase*

The temperature dependence of the $\nu_i$ is very unusual. While $\nu_1$ and $\nu_4$ approach zero for $T \rightarrow T_c$, as expected, $\nu_1(T)$ in particular scales very well with the magnetization of the

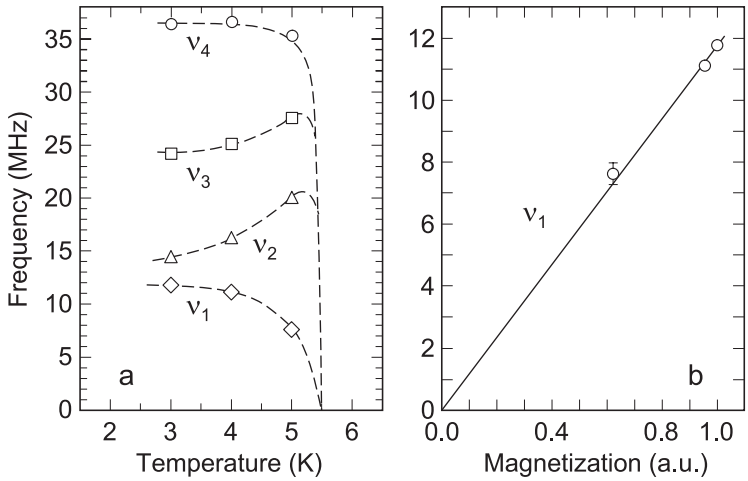


**Figure 9.** (a) The temperature dependence of the four spontaneous precession frequencies $\nu_i$ below $T_c$. The dashed curves are guides to the eye. (b) A plot of $\nu_1$ versus saturation magnetization [4].

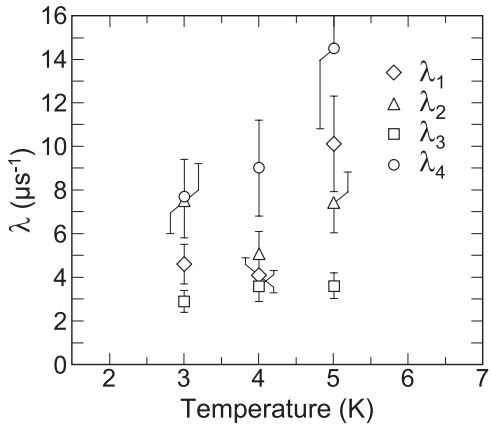


**Figure 10.** The temperature dependence of the relaxation rates $\lambda_i$ ($i = 1, 2, 3$) (equation (9)) below $T_c$.

sample (see figure 9(b)) and $\nu_2$ and $\nu_3$ show an increase with increasing temperature. The trend of $\nu_i(T)$ suggests that at 3 K the $\nu_i$ are already close to saturation. At 3 K the four frequencies correspond to internal fields of $B_1 = 0.87 \pm 0.07$ kG, $B_2 = 1.07 \pm 0.22$ kG, $B_3 = 1.79 \pm 0.05$ kG and $B_4 = 2.68 \pm 0.22$ kG (see also table 3). For a ferromagnet with zero net magnetization the internal field is given by [16]

$$\boldsymbol{B}_i = \frac{4\pi}{3}\boldsymbol{M}_d + \boldsymbol{B}_{dip} + \boldsymbol{B}_c, \tag{10}$$

where the first term is the Lorentz field and $\boldsymbol{M}_d$ the domain magnetization, $\boldsymbol{B}_{dip}$ the total dipole field from the ordered Ce 4f moments and $\boldsymbol{B}_c$ the contact hyperfine field due to the spin polarization of the conduction electrons at the $\mu^+$ position. According to [4, 5] $M_d$ is of the order of 1 $\mu_B$/Ce $= 8.58 \times 10^3$ emu mol$^{-1}$ $= 0.173 \times 10^3$ emu cm$^{-3}$ and hence $(4\pi/3)M_d \simeq 0.725$ kG, directed parallel to the tetragonal $c$-axis [3]. An effectively ferromagnetic arrangement of the Ce moments was also realized in the TF measurements in

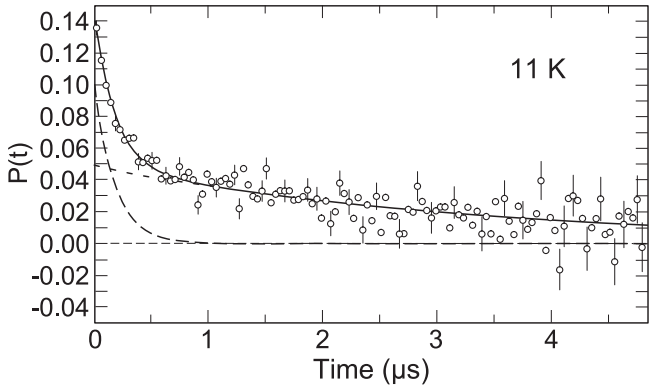


**Figure 11.** The time dependence of the $\mu^+$ polarization $P(t)$ in ZF at 11 K in the 'forward' direction. The solid curve represents a fit of equation (12) to the data; the dashed curves show the individual contributions of the two components.

the paramagnetic state and the corresponding coupling constants, appropriate for the c site, are listed in tables 1 and 2. Accordingly we may write

$$\boldsymbol{B}_{\rm hf} = \boldsymbol{B}_{\rm dip} + \boldsymbol{B}_{\rm c} = (\overleftrightarrow{A}_{\rm dip} + A_{\rm c})\boldsymbol{\mu}, \tag{11}$$

where $\boldsymbol{\mu}$ is parallel to the $c$-axis and so are $\boldsymbol{B}_{\rm dip}$ and $\boldsymbol{B}_{\rm c}$; i.e. the Lorentz field $\frac{4\pi}{3}\boldsymbol{M}_{\rm d}$, $\boldsymbol{B}_{\rm dip}$ and $\boldsymbol{B}_{\rm c}$ are collinear. However, we do not know the sign of the $\boldsymbol{B}_i$ relative to the Lorentz field. Hence $B_{{\rm hf},i} + M_{\rm d} = \pm B_i$ and $B_{{\rm hf},i} = \pm B_i - M_{\rm d}$. The possible values for $B_{{\rm hf},i}$ at 3 K are collected in table 3. Since the ordered moment is of order 1 $\mu_{\rm B}$ the values listed for $B_{{\rm hf},i}$ nearly correspond to $A_{{\rm dip},i} + A_{{\rm c},i}$ (kG/$\mu_{\rm B}$). Assigning the various frequencies unambiguously to particular sites is not possible. However, we think that $\nu_1$ is associated with the defect site since it is the only frequency which scales with the magnetization or the ordered moment, while the three other frequencies display an anomalous behaviour. Moreover, if we believe that the defect site is a vacancy, then $B_{\rm hf} = B_{\rm c}$ and we extract a contact coupling constant of $-0.64$ kG/$\mu_{\rm B}$ at 3 K which is not drastically different from $A_{\rm c} = -0.33$ kG/$\mu_{\rm B}$ at 6 K derived from $K_4(T)$.

Independently of the choice of the sign of $\boldsymbol{B}_i$ ($i = 2, 3, 4$) relative to $\boldsymbol{M}_{\rm d}$ and the assignment of the $\nu_i$ to a particular c site, we find that the contact coupling constant $A_{\rm c}(T) = B_{\rm c}(T)/\mu(T)$ has to rise with increasing temperature when $T_{\rm c}$ is approached in order to reproduce $\nu_i(T)$. A possible choice is to assign $\nu_2$ to the site $(0\frac{1}{2}\frac{1}{2})$, $\nu_3$ to $(\frac{1}{2}0\frac{1}{2})$ and $\nu_4$ to $(\frac{1}{2}\frac{1}{2}0)$ and to assign a negative sign to $B_2$, $B_3$ and $B_4$. With this choice we extract the $A_{\rm c}$ values displayed in figure 7 and table 3. At least $A_{\rm c}$ for the $(0\frac{1}{2}\frac{1}{2})$ site seems to show a smooth increase in absolute value from 3 K up to high temperatures. For the other two sites an abrupt change of $A_{\rm c}$ at $T_{\rm c}$ is indicated. From the $A_{\rm c}$ values at 3 K we calculate $A^{\rm c}_{i'i'}$ values listed in table 4. As can be seen, they are vastly different from the corresponding values for $T \gtrsim 10$ K. Similar results are found for other choices, demonstrating that some of the contact coupling parameters are strongly modified by the ferromagnetic phase transition in contrast to the absence of any anomalies at $T_{\rm Q}$.

### *4.3. The ferroquadrupolar phase ($T_c < T < T_Q$) and the paramagnetic phase ($T > T_Q$)*

The ZF signal in all four directions (forward, backward, up, down) for $T_{\rm c} < T < T_{\rm Q}$ is now composed of two components and best fitted by the expression (see figure 11)

$$P(t) = A_1 \exp(-\lambda_1^* t) + A_2 \exp(-\lambda_2^* t), \tag{12}$$

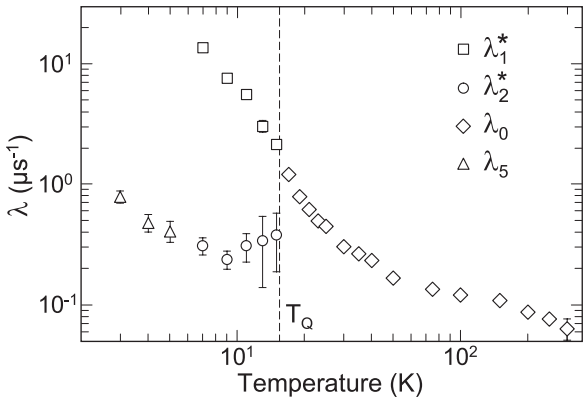


**Figure 12.** A log–log plot of the temperature dependence of $\lambda_5$ (equation (9)), $\lambda_1^*$ and $\lambda_2^*$ (equation (12)) and $\lambda_0$ (equation (14)).

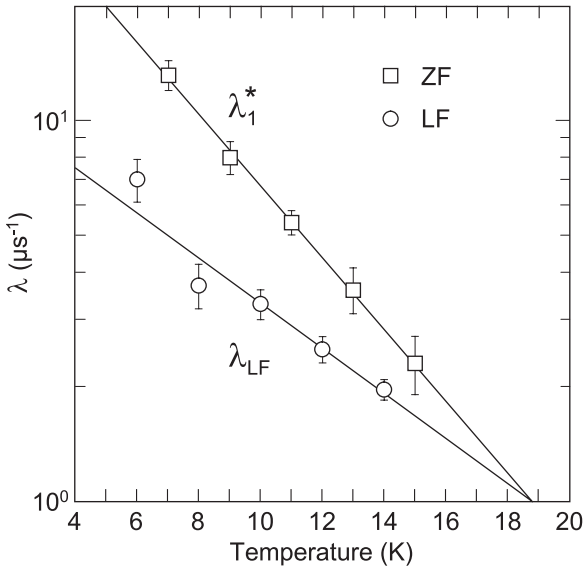


**Figure 13.** A semi-logarithmic plot of $\lambda_1^*$ and $\lambda_{LF}$ below $T_Q$. The solid lines represent fits of equation (13) to the data.

with $A_2 = \frac{1}{2}A_1$, where $A_1 + A_2$ corresponds to the full $\mu^+$ beam polarization; i.e. all implanted $\mu^+$ contribute to the signal. The temperature dependence of the fitted $\lambda_1^*$ and $\lambda_2^*$ is displayed in figure 12. The ratio $A_1/A_2 = 2$ could indicate that the first component reflects random static fields with a Lorentzian distribution and the second component those $\mu^+$ whose spin happens to be oriented along the static internal fields (the so-called 1/3 component). However, in view of the LF results (see section 5), it appears that the first, fast relaxing component also reflects dynamically induced depolarization.

The temperature dependence of $\lambda_1^*$ is found to follow an exponential behaviour:

$$\lambda_1^* = \lambda_1^*(0)\exp(-T/E), \tag{13}$$

with $E = 9.23 \pm 0.85$ K and $\lambda_1^*(0) = (5.8 \pm 1.2) \times 10^7$ s$^{-1}$ (see figure 13). No diverging behaviour on approaching $T_c$ is evident.

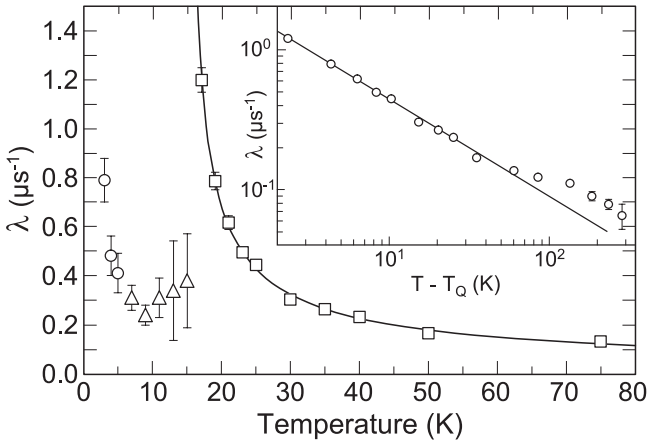


**Figure 14.** Linear plots of $\lambda_5$, $\lambda_2^*$ and $\lambda_0$ versus temperature. The solid curve represents a fit of equation (15) to the $\lambda_0$ values. The inset shows $\log \lambda_0$ versus $\log(T - T_Q)$.

Just above $T_Q$ the ZF signal reduces to a single exponentially relaxing component:

$$P(t) = A_0 \exp(-\lambda_0 t), \tag{14}$$

with $A_0 = A_1 + A_2$. The temperature dependence of $\lambda_0$ is plotted in figure 12 as well. Obviously, above $T_Q$, the $\mu^+$ are exposed to random and isotropically fluctuating fields. The most remarkable aspect is that $\lambda_0$ displays a diverging behaviour on approaching $T_Q$ from above which reflects a (critical?) slowing of the $Ce^{3+}$ spin dynamics preceding the onset of the ferroquadrupolar order. In the range 16 K $\leqslant T \leqslant$ 70 K, $\lambda_0(T)$ is excellently fitted by the equation (see figure 14)

$$\lambda_0(T) = \frac{\lambda_0}{(T - T_{cri})^\beta} \tag{15}$$

with $\beta = 0.70 \pm 0.04$ and $T_{cri} = 14.7 \pm 0.4$ K. $T_{cri}$ is very close to $T_Q = (15\text{–}16)$ K and may be identified with $T_Q$. The (critical) exponent $\beta$ may be compared with the prediction for a 3D Heisenberg system, admitting non-spin-conserving dipole–dipole interactions: $\beta = 0.705$ [17]. The agreement is striking, but may be fortuitous.

### *4.4. Discussion of the ZF result above $T_c$*

The ZF results obtained imply a strong coupling of the $Ce^{3+}$ spin dynamics and the quadrupolar order. Not only is the spin dynamics slowed down in preparation for the ferroquadrupolar state, but the spin dynamics below $T_Q$ displays a separation into a fast and a slow regime with a population of 2:1. This behaviour can be understood if we assume that below $T_Q$ the 4f moments start to fluctuate in a ferromagnetically correlated manner, e.g. along one of the crystal axes, which transform to the tetragonal $c$-axes below $T_Q$.

The initial $\mu^+$ polarization components in the forward–backward direction and in the up–down direction will relax if the fluctuating fields are perpendicular to these components. If they are parallel, strictly no depolarization should occur. The latter situation is realized for $1/3$ and the former situation for $2/3$ of the implanted $\mu^+$; this is the case for each component separately. The small residual polarization of the $1/3$ component may arise from a small remaining and fluctuating 4f moment component perpendicular to the $c$-axes or a small misalignment of the sample. Hence it appears that the ferroquadrupolar order restricts the degrees of freedom of

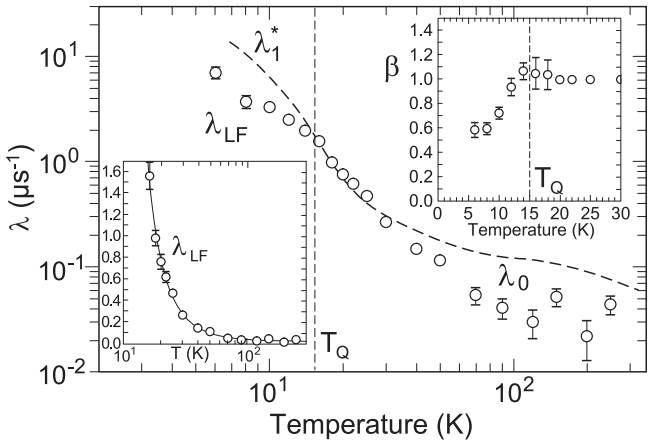


**Figure 15.** A log–log plot of the temperature dependence of $\lambda_{LF}$. $\lambda_1^*$ and $\lambda_0$ are represented by the dashed curve. The inset in the upper right corner displays $\beta(T)$ (equation (16)), the inset in the lower left corner $\lambda_{LF}$ versus $\log(T)$. The solid curve in this inset represents a fit of equation (15) to the data.

the 4f moments to the tetragonal *c*-axes. In a certain sense the magnetic state below $T_Q$ can be viewed as a precursor to the ferromagnetic phase. The final transition into the ferromagnetic state will not cost much energy and may be of first order in zero applied field. This could explain the absence of a diverging behaviour of $\lambda_1^*$ on approaching $T_c$.

## 5. Measurements in longitudinal field

As described in section 2, in the spin-rotated configuration one can simultaneously observe the $\mu^+$ Larmor precession and the $\mu^+$ spin–lattice relaxation in the applied field $H_{ext}$. In our experiment $H_{ext} = 6$ kOe and $\boldsymbol{H}_{ext} \parallel [100]$ crystal axis. In the whole temperature range $6\ \mathrm{K} < T < 250\ \mathrm{K}$ investigated, the LF signal consisted of only one component which below $T_Q$ was best fitted by a stretched exponential decay function

$$P(t) = A_0 \exp(-(\lambda_{LF} t)^{\beta}), \tag{16}$$

and above $T_Q$ by equation (14). The fit results as a function of temperature are displayed in figure 15. As can be seen, $\beta$ changes from 0.5 near $T_c$ to 1 for $T \to T_Q$ (the inset in figure 15) and $\lambda_{LF}$ displays an inflection point at $T_Q$. The asymmetry $A_0$ shows no temperature dependence from 6 up to 250 K. In figure 15 we also include the temperature dependence of $\lambda_1^*$ and $\lambda_0$, represented by the dashed line. As can be seen, $\lambda_{LF} \simeq \lambda_0$ for $T$ in the range from $T_Q$ to 30 K. Below $T_Q$, $\lambda_{LF}$ is not dramatically smaller than $\lambda_1^*$. We take this as evidence that $\lambda_1^*$ is of dynamic origin and not arising from a distribution of static fields, from which the $\mu^+$ spins should be decoupled in $H_{ext} = 6$ kOe. The absence of a field dependence in the range $T_Q$ to 30 K suggests on the basis of the Redfield formula [10] that $\omega\tau_c \ll 1$, where $\omega$ is the $\mu^+$ Zeeman frequency. In this case

$$\lambda_{LF} = \gamma_\mu^2 B_\perp^2 \tau_c \tag{17}$$

where $\tau_c^{-1}$ is the fluctuation rate and $B_\perp$ the fluctuating field amplitude at the $\mu^+$. Assuming that $B_\perp$ is of the same order as the spontaneous fields below $T_c$, i.e. $\langle B_\perp \rangle \approx 1.6$ kG, we estimate that at $\sim T_Q$ ($\lambda_{LF} \simeq 1.5 \times 10^6\ \mathrm{s}^{-1}$), $\tau_c \simeq 8 \times 10^{-11}$ s or $\tau_c^{-1} \simeq 1.2 \times 10^{10}\ \mathrm{s}^{-1}$, consistent with the condition $\omega\tau_c \ll 1$ at $H_{ext} = 6$ kOe. Below $T_Q$, $\lambda_{LF}$ becomes smaller than $\lambda_1^*$ and it is

reasonable to assume that this deviation can be attributed to the term $\omega\tau_c$, which is no longer negligibly small compared with 1, so [10]

$$\lambda = \gamma_\mu^2 B_\perp^2 \frac{\tau_c}{1+\omega^2\tau_c^2} \tag{18}$$

has to be considered. With $\lambda_{LF} = 7 \times 10^6$ s$^{-1}$ at 6 K we estimate $\tau_c \simeq 3.9 \times 10^{-10}$ s ($\tau_c^{-1} \simeq 2.8 \times 10^9$ s$^{-1}$); i.e. the spin dynamics has not slowed down much from $T_Q$ to near $T_c$.

$\lambda_{LF}(T)$, like $\lambda_1^*(T)$, displays below $T_Q$ an exponential temperature dependence (equation (13)) with fitted $E = 14.7 \pm 2.0$ K (see figure 13). Given the error bars, this result coincides essentially with the corresponding ZF value. The observation of only a one component signal points also to a restoration of random, isotropically fluctuating fields below $T_Q$, and the stretched exponential relaxation points to a distribution of relaxation rates [18], all signalling a suppression of the ferromagnetically correlated fluctuations below $T_Q$ by the applied field.

As regards the temperature range above $T_Q$, we find that $\lambda_{LF}(T)$ from 16 up to 250 K is also well fitted by equation (15) (see the inset in figure 15) with $T_{cri} = (3.5 \pm 4.5)$ K, unlike the case in ZF. Fixing $T_{cri} = T_c = 5.5$ K, one obtains $\beta = 2.1(1)$ as compared to $\beta = 0.70$ in ZF. It appears that in LF for $T > T_Q$ the freezing of the 4f moment dynamics is preparing to happen at $\sim T_c$, while in ZF this is at $T_Q$. But this trend is suppressed below $T_Q$ and, instead, $\lambda_{LF}(T)$ shows an inflection point at $T_Q$. It would be interesting to extend these measurements to higher fields, since the Zeeman interaction of the 4f moments and the quadrupolar order seem to compete in their effect on the 4f spin dynamics.

## 6. Summary and conclusions

The present work on CeAg has demonstrated once more that quadrupolar effects can be monitored by $\mu$SR spectroscopy under ZF, LF and TF conditions and that new features are revealed. In particular it is found that the conduction electron spin polarization responds in a characteristic way to the presence of aspherical charge distributions of f electrons (or quadrupole moments) manifested by pronounced anisotropic and unusual temperature dependent contact hyperfine fields at the $\mu^+$. The anisotropy is not restricted to the regime of quadrupolar order but is visible also at higher temperatures. These features are suggested to arise from the RKKY mechanism which becomes anisotropic in the presence of quadrupole moments when the overlap integral of the aspherical f electron charge distribution and the conduction electrons depends on the orientation of the quadrupole moment. In the present case, the anisotropy of the contact hyperfine coupling constant extracted from the $\mu^+$ Knight shift can be phenomenologically reproduced by assuming that the quadrupole moment can be aligned by an external field (6 kOe in our case), implying strong $LS$ coupling. It is also found that the onset of the ferromagnetic order below $T_c \simeq 5.5$ K abruptly modifies the anisotropy of the contact coupling constant. No such change is seen at $T_Q$, in contrast to the case for $CeB_6$ [15], which is understandable if, in the presence of an external field $\boldsymbol{H}_{ext}$, only a single ferroquadrupolar domain is formed with the tetragonal axis parallel to $\boldsymbol{H}_{ext}$.

The muon spin–lattice relaxation rate was studied in ZF and LF. The ZF results imply random and isotropic fluctuations of the 4f moments above $T_Q$, but the fluctuations show a (critical) slowing down upon approaching $T_Q$ as if the Ce sublattice already wanted to order magnetically at $T_Q$. Crossing below $T_Q$, the onset of the ferroquadrupolar order apparently blocks the development of magnetic order and the data imply instead a transition of the isotropic fluctuations to ferromagnetically correlated fluctuations along the tetragonally distorted axes. This is consistent with our assertion that the quadrupole moment and the magnetic dipole

moment are strongly coupled together. This behaviour appears suppressed in a LF of 6 kOe which restores the isotropic fluctuations but leads to spatially inhomogeneous relaxation rates. Approaching $T_c$, neither in ZF nor in LF did the muon spin–lattice relaxation rate reveal any divergent or critical behaviour, indicating that the transition into the ferromagnetic phase is of first order.

Finally, below $T_c$, the $\mu$SR signal reveals the presence of spontaneous internal fields with a multiplicity which corresponds to the threefold splitting of the TF $\mu$SR signal above $T_c$ and is attributed to the occupation of the interstitial 3c sites. The partially anomalous temperature dependence of the spontaneous frequencies is traced back to the contact hyperfine field and an anisotropic and temperature dependent contact coupling constant as mentioned above. A small fourth signal, both in the TF data above $T_c$ and in the ZF data below $T_c$, is suggested to arise from $\mu^+$ located at a vacancy in the Ag sublattice.

It is interesting to compare the present findings with $\mu$SR results for other compounds exhibiting quadrupolar order. The effect of a non-spherical f electron charge distribution on the RKKY mechanism and the induced conduction electron spin polarization has been observed also in $UPd_3$ [13], $HoB_2C_2$ [14], $CeB_6$ [15] and possibly $PrCu_2$ [19]. In $UPd_3$ it was primarily revealed by the development of an inhomogeneous conduction electron spin polarization below the onset temperature of antiferroquadrupolar order, and in the three other compounds via the contact contribution to the Knight shift. Similar Knight shift results obtained for $U_{0.965}Th_{0.035}B_{13}$ [12] suggest that U in this compound also carries a quadrupole moment. The effect of quadrupolar order on the f electron spin dynamics is so far unique to CeAg. For $PrCu_2$ the observed high temperature magnetic order is explained as being driven by a partial freezing of the quadrupolar degrees of freedom, concurrent strain and resulting magneto-elastic coupling. In the latter case it was also suggested that fluctuations of the quadrupole moments can give rise to fluctuating contact hyperfields which in turn cause the $\mu^+$ spin polarization to relax. Looking at the results in detail, it appears that each compound mentioned reflects the presence of quadrupole moments differently, testifying to the richness of side effects accompanying the presence of aspherical f electron charge distributions: anisotropic and inhomogeneous conduction electron spin polarization, freezing of quadrupolar degrees of freedom, coupling of dipole and quadrupole moments, the effect on the f electron spin dynamics and spin–lattice relaxation induced by stochastic rotational motions of the quadrupole moments. The results on CeAg illuminate some of those side effects. A direct observation of quadrupolar order by means of $\mu$SR is, of course, not possible.

## Acknowledgments

We thank the staff at the Laboratory for Muon-Spin Spectroscopy (S$\mu$S), in particular Dr A Amato, responsible for the GPS instrument, and the proton accelerator crew of the Paul Scherrer Institute (PSI) for providing excellent measuring conditions.

## References

[1] Morin P and Schmitt D 1990 *Ferromagnetic Materials* vol 5, ed K H J Buschow and E P Wohlfarth (Amsterdam: North-Holland)
[2] Morin P 1988 *J. Magn. Magn. Mater.* **71** 151
[3] Schmitt D, Morin P and Pierre J 1978 *J. Magn. Magn. Mater.* **8** 249
[4] Takke R, Dolezal N, Assmus W and Lüthi B 1981 *J. Magn. Magn. Mater.* **23** 247
[5] Sato H, Sugawara H, Aoki Y, Motoki K, Settai R and Ōnuki Y 1996 *J. Phys. Soc. Japan* **65** 1329
[6] See e.g. Lee S L, Cywinski R and Kilcoyne S H (ed) 1999 *Muon Science (Scottish Universities Summer Schools in Physics 51)* (Bristol: Institute of Physics Publishing)

[7] Hyomi K, Amitsuka H, Nishioka T, Marayama S, Miyako Y, Nishiyama K, Nagamine K, Yamazaki T and Morin P 1988 *J. Magn. Magn. Mater.* **76+77** 462
[8] Motoki K, Settai R, Kimura N, Toshima H, Ebihara T, Ikezawa H, Sugawara H, Ōnuki Y and Harima H 1995 *J. Phys. Soc. Japan* **64** 3328
[9] Alexandrowicz G, Tashma T, Socolovsky M, Amato A, Grayevski A, Gygax F N, Pinkpank M, Schenck A and Kaplan N 1999 *Phys. Rev. Lett.* **82** 1028
[10] Slichter C P 1978 *Principles of Magnetic Resonance* (Berlin: Springer)
[11] See e.g. Schenck A 1999 *Muon Science (Scottish Universities Summer Schools in Physics 51)* ed S L Lee, R Cywinski and S H Kilcoyne (Bristol: Institute of Physics Publishing)
[12] Sonier J E, Heffner R H, McLaughlin D E, Nieuwenhuys G J, Bernal O, Movshovich R, Pagliuso P G, Cooley J, Smith J L and Thompson J D 2000 *Phys. Rev. Lett.* **85** 2821
[13] Schenck A, Gygax F N and McEwen K A 2002 *J. Phys.: Condens. Matter* **14** 4595
[14] De Lorenzi F, Gygax F N, Schenck A, Tobo A and Onodera H 2003 *Physica* B **326** 581
[15] Schenck A *et al* 2002 *Phys. Rev. Lett.* **89** 037201
Schenck A *et al* 2003 to be published
[16] Kalvius G M, Noakes D R and Hartmann O 2001 *Handbook on the Physics and Chemistry of Rare Earths* vol 32, ed G H Lander, K A Gschneidner Jr and Le R Eyring (Amsterdam: Elsevier Science)
[17] See e.g. Yaouanc A, Dalmas de Réotier P and Frey E 1993 *Phys. Rev.* B **47** 796
[18] Kalvius G M, Noakes D R and Hartmann O 2001 *Handbook on the Physics and Chemistry of Rare Earths* vol 32, ed G H Lander, K A Gschneidner Jr and Le R Eyring (Amsterdam: Elsevier Science) section 3.2.2
[19] Schenck A, Gygax F N and Ōnuki Y 2003 *Phys. Rev.* B **68** 1004422